

Measurement of the space-time extent of the hard-photon emitting source in heavy-ion collisions at 100 MeV/nucleon

A. Badalà,¹ R. Barbera,^{1,2} A. Palmeri,¹ G. S. Pappalardo,¹ F. Riggi,^{1,2} G. Rizza,² A. C. Russo,¹ G. Russo,^{2,3} and R. Turrisi^{1,2}

¹*Istituto Nazionale di Fisica Nucleare, Sez. di Catania, Corso Italia, 57-I 95129 Catania, Italy*

²*Dipartimento di Fisica dell'Università di Catania, Corso Italia, 57-I 95129 Catania, Italy*

³*Istituto Nazionale di Fisica Nucleare, Laboratorio Nazionale del Sud, Via Santa Sofia, 44-I 95123 Catania, Italy*

(Received 10 January 1997)

The correlation between the couples of high-energy photons ($E_\gamma > 30$ MeV) detected in the reactions induced by a ^{36}Ar beam on ^{27}Al , ^{112}Sn , and ^{197}Au targets at 95 MeV/nucleon has been analyzed with the intensity interferometry technique. Both the size and lifetime of the emitting source have been quantitatively evaluated. Results support the nucleon-nucleon picture as the dominant hard-photon production mechanism. [S0556-2813(97)05905-0]

PACS number(s): 25.70.-z, 13.75.Cs

I. INTRODUCTION

The present availability of large-area and high-granularity detectors for high-energy photons emitted in heavy-ion reactions at intermediate energies has permitted, in recent years, the use of the intensity interferometry technique [1] in the study of the space-time characteristics of the emitting source [2]. This is not of trivial importance since such a method of analyzing photon-photon correlations can be used as a model-independent tool to shed light, in a definitive manner, on the hard-photon production mechanism and time scale. Unfortunately, the very small cross sections associated with the presence of the many sources of a rather large background, such as neutral pion decays and cosmic-ray interactions with the detector, do not allow a direct and comparative study of multidimensional correlation functions. Also, the evaluation of the space-time characteristics of the source is not straightforward at all. Furthermore, a very detailed knowledge of the response function of the used detector to the couples of correlated photons and to the sources of noise is of crucial importance to extract reliable values of the emitting source parameters to be compared with the existing theoretical models.

In this paper we present an extensive application of the intensity interferometry technique to the pairs of high-energy photons ($E_\gamma > 30$ MeV) emitted in the reactions induced by a ^{36}Ar projectile on ^{27}Al , ^{112}Sn , and ^{197}Au targets at 95 MeV/nucleon. The presentation and discussion of the experimental results are preceded by the description of a new analysis method permitting the simultaneous determination of both spatial and time extensions of the source through the study of monodimensional correlation functions. Moreover, much attention has been devoted throughout the paper to a deep analysis of the influence of the real detector limitations (both geometric and intrinsic) on the quantitative evaluation of the photon-photon correlation.

The paper is organized as follows. Section II contains a description of the used experimental setup. Section III is devoted to the study of the detector response both to the correlation signal and to the sources of background. Results are

presented in Sec. IV. A summary and conclusions are given in Sec. V.

II. EXPERIMENTAL SETUP

The experiment was performed at the GANIL facility, irradiating ^{27}Al (1.6 mg/cm²), ^{112}Sn (0.8 mg/cm²), and ^{197}Au (4.1 mg/cm²) targets with a 95-MeV/nucleon ^{36}Ar beam.

A. Generalities

The experimental setup used basically consisted of the BaF₂ ball of the MEDEA multidetector (see Fig. 1). It is made up of 144 trapezoidal scintillation modules of barium fluoride (20 cm thick) placed at 22 cm from the target point and arranged into six rings to cover the whole azimuthal angular dynamics between $\theta = 40^\circ$ and $\theta = 140^\circ$ with respect to the beam direction. The whole subtended solid angle is about 10 sr over a useful surface of 0.55 m². A very detailed description of this multidetector can be found in Ref. [3].

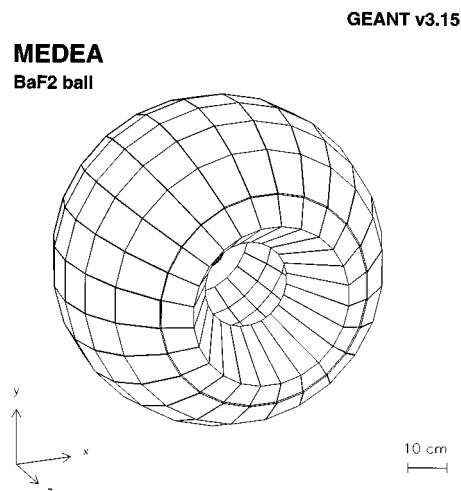


FIG. 1. Global view of the BaF₂ ball of the MEDEA multidetector.

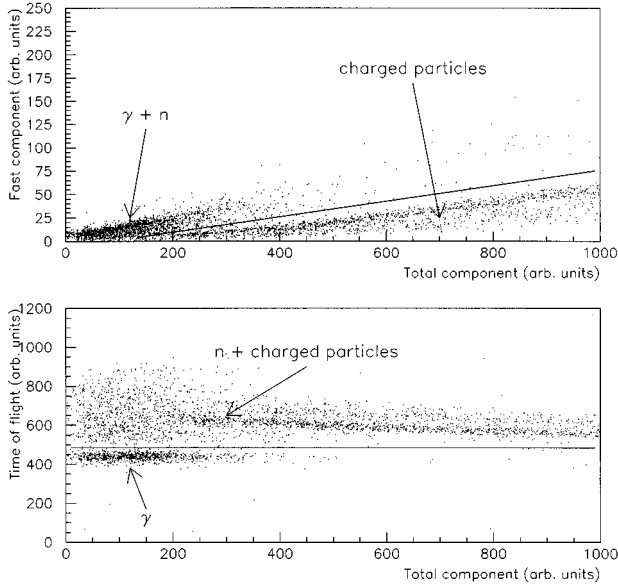


FIG. 2. Fast component of the analogic signal vs total component of the analogic signal (upper panel), and time of flight vs total component of the analogic signal (lower panel) for particles, coming from the reaction $^{36}\text{Ar}+^{27}\text{Al}$ at 95 MeV/nucleon, and detected by one module of the BaF_2 ball of the MEDEA multidetector. In both figure lines refer to the separation between neutral particles (photons and neutrons) and charged particles.

B. Photon identification

High-energy photons have been selected and identified by means of the usual shape analysis of the analog signal coupled with the time-of-flight (TOF) information. The start for the TOF was given by the accelerator rf and the total time resolution was about 800 ps. The capability of a single detection module (taken as an example) of separating γ rays from neutrons and other charged particles is shown in Figs. 2 and 3 which are relative to the ^{27}Al target. The energy calibration for photons has been carried out using both a 6.13 MeV γ -ray PuC source and the value of the energy deposited by cosmic rays traversing two opposite detectors all along their longest side. The energy dynamics in which photons have been detected and identified spans from about 20 MeV to 230 MeV but only those having an energy strictly greater than 30 MeV have been considered in the present analysis. Only those 2γ events where two photons were detected in coincidence with at least two charged particles have been kept. This condition has been imposed to reduce to a negligible amount the background induced by cosmic radiation (see Sec. II B 3).

C. Neutral pion identification

In addition to high-energy photons, also neutral pions have been detected in the same experiment. They have been recorded in the whole solid angle and in the kinetic energy range between zero and about 120 MeV through the simultaneous detection of the couples of photons coming from their main decay mode [$\pi^0 \rightarrow 2\gamma$, branching ratio (BR) = 98.8%]. These photons are separated from others by imposing severe conditions on the experimental distributions of the relative angle θ_{12} and invariant mass m_{inv} as functions of

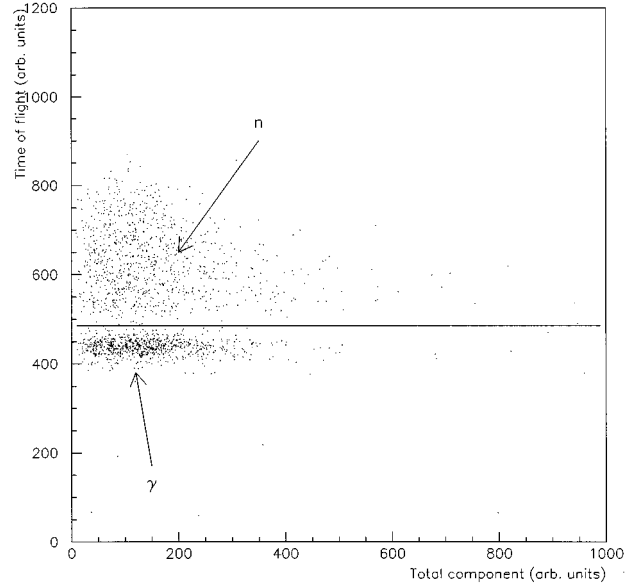


FIG. 3. Time of flight vs total component of the analogic signal for neutral particles (staying above the line in Fig. 2, upper panel), coming from the reaction $^{36}\text{Ar}+^{27}\text{Al}$ at 95 MeV/nucleon, and detected by one module of the BaF_2 ball of the MEDEA multidetector. The line refers to the separation between photons and neutrons.

the total energy $E_1 + E_2$ of the two detected photons which are reported, for the ^{27}Al target, in the upper panel and in the lower panel of Fig. 4, respectively. The cuts drawn in both panels of Fig. 4 select those photons coming from π^0 decay. They were chosen following the results of full GEANT3 [4] simulations performed to determine the detector efficiency as a function of the pion kinetic energy and detection angle (see

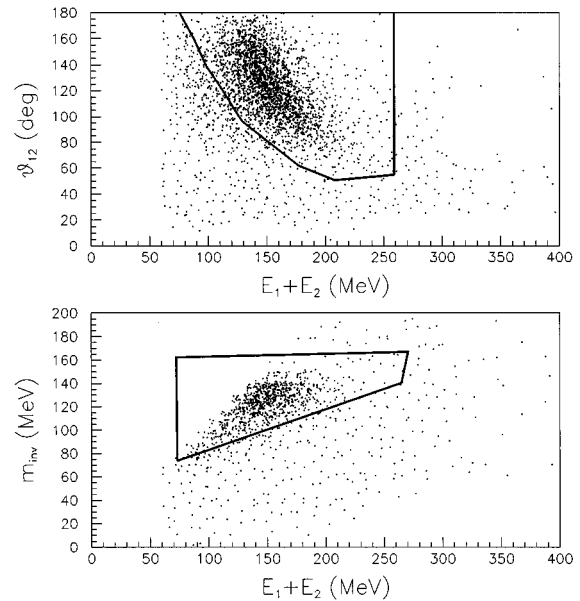


FIG. 4. Relative angle (upper panel) and invariant mass (lower panel) versus total energy distributions of the pairs of photons detected in the reaction $^{36}\text{Ar}+^{27}\text{Al}$ at 95 MeV/nucleon. In both plots, the contours define those pairs of photons coming from π^0 decay.

the next section). The performances of the MEDEA multidetector as a photon and neutral pion spectrometer for the same experiment discussed in this paper have already been published in Refs. [5, 6]. Although many results will be reported in the following, the reader is referred to those papers for more details.

III. RESPONSE OF THE DETECTOR

Before even thinking about the realization of an experiment based on the Hanbury-Brown–Twiss (HBT) effect, it is of fundamental importance to precisely know the response of the detector to be used both for the correlation signal one wants to observe and to the background one expects to have. In this section we present the results of a study of the response of BaF₂ ball of the MEDEA multidetector performed by means of full GEANT3 [4] simulations. Further details on the analysis procedure have been also discussed in Refs. [7–9].

A. Response to the signal

1. Single photons

The γ rays are detected in the BaF₂ ball of MEDEA simply by means of the calorimetric collection of the electromagnetic showers they induce into the detector material. The determination of the energy and angles of the detected photons is carried out using the following procedure. All modules having a value of the deposited energy different from zero are scanned in order to find the “most-touched” detector (i.e., the one with the highest value of the deposited energy). Let us call it (i_{\max}, j_{\max}) , where the index i ($i=1,2,\dots,24$) is an order parameter running over the elements of one ring and the index j ($j=1,2,\dots,6$) is an order parameter running over the useful rings of the ball (the six most-backward ones). When this detector is found the analysis code looks at all detectors verifying the relation $(i_{\max}-i)^2+(j_{\max}-j)^2 \leq 2$ in order to determine whether or not the electromagnetic shower spreads out in these neighboring modules. If none with a deposited energy greater than its threshold is found, the photon energy is fixed equal to the deposited energy in the central detector and the polar and azimuthal detection angles are uniformly randomized within that detector. Otherwise, as is mostly the case, the energy of the photon-induced shower is obtained by summing over all elements of the cluster and the photon detection angles are evaluated as the averages of the corresponding (randomized) angles of the single detectors of the cluster, weighted over the deposited energy in each cluster element. When the energy and the detection angles of the first shower are determined and the shower multiplicity is greater than 1, the first “most-touched” detector and the involved neighboring modules are excluded from the loop and the program starts again to find a new “most-touched” detector. As has been shown in Refs. [3,7], this kind of procedure minimizes the sideward leakages of the shower (the full side dimension of each detection module is nearly twice the Molière radius of barium fluoride), ensuring a good estimate of the detector response to photons. It introduces, however, a lower threshold in the relative angle between two simultaneously detected photons of about 15°. In order to considerably reduce

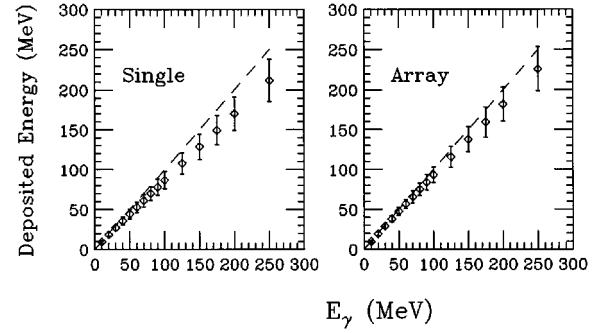


FIG. 5. Mean value of the deposited energy in the central detector (single module of the BaF₂ ball) and in the cluster as it has been defined in the text, as a function of the incoming photon energy. The dashed line is the linear (ideal) dependence. Error bars indicate one-rms deviations.

the background due to neutrons, the condition that the energy deposited in the central detector only must be larger than 20 MeV is also applied to the data.

Figure 5 shows the mean value of the deposited energy, as a function of the incident photon energy, in the case (a) where one considers one single module (left panel) and in the case (b) where one considers a complete cluster (right panel). When the energy deposited in the neighboring detectors is properly included in the sum, the trend is more linear, approaching the ideal dependence, given by the dashed line. One rms deviation is reported as an error bar on the data. Moreover, to give an idea of the degree of accuracy in the knowledge of the detector efficiency for photons, in Fig. 6 the comparison between an input Boltzmann-like spectrum and that reconstructed after filtering through the detector is shown.

2. Correlated photons

The correlation function between two photons, having wave vectors \vec{k}_1 and \vec{k}_2 , is defined as [10,11]

$$F^{id}(\vec{k}_1, \vec{k}_2) \equiv \frac{P(\vec{k}_1, \vec{k}_2)}{P(\vec{k}_1)P(\vec{k}_2)} = N \frac{d^6 n}{d^3 k_1 d^3 k_2} /$$

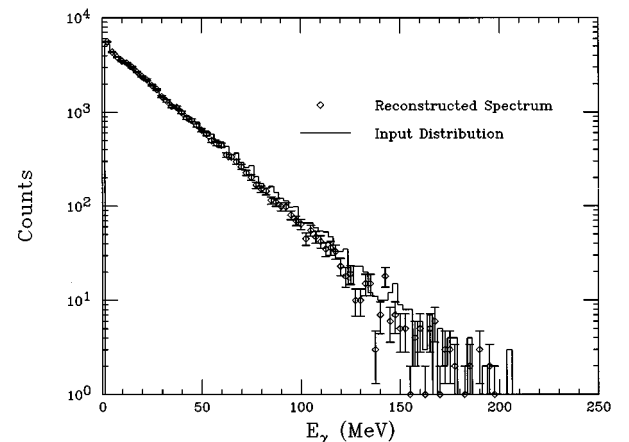


FIG. 6. Comparison between an input Boltzmann-like photon spectrum and that reconstructed after filtering through the detector.

$$\left. \frac{d^3n}{d^3\vec{k}_1} \frac{d^3n}{d^3\vec{k}_2} \right), \quad (1)$$

where $P(\vec{k}_{1,2})$ and $P(\vec{k}_1, \vec{k}_2)$ are the one-photon and two-photon inclusive distributions, respectively. The factor N in Eq. (1) follows from the relative normalization of these distributions. Taking into account the polarization of the photons and assuming that (i) the coherent electromagnetic current can be neglected, (ii) all neutron-proton collisions produce the same magnitude of electromagnetic current, and (iii) currents from different collisions have uncorrelated directions, Neuhauser has shown [11] that the two-photon correlation function assumes the form

$$\begin{aligned} F(\vec{k}_1, \vec{k}_2) &= 1 + \frac{1}{2} [1 + (\hat{\mathbf{k}}_1 \cdot \hat{\mathbf{k}}_2)^2] \times \frac{1}{2} [|\rho(k_1 + k_2)|^2 \\ &\quad + |\rho(k_1 - k_2)|^2] \\ &\equiv 1 + C_2(\vec{k}_1, \vec{k}_2), \end{aligned} \quad (2)$$

where $\hat{\mathbf{k}}_1$ and $\hat{\mathbf{k}}_2$ are unit vectors along the directions of the two photons and $\rho(k)$, as a function of the four-vector k , is the four-dimensional Fourier transform of the normalized space-time density $\rho(\vec{r}, t)$ of the photon source. The term $[1 + (\hat{\mathbf{k}}_1 \cdot \hat{\mathbf{k}}_2)^2]$, which reduces the maximum value of the correlation function from 2 to 1.5, is due to the photon polarization [11] and takes into account that orthogonally polarized photons cannot interfere. If the energies of both correlated photons are sufficiently high ($E_{\gamma_1}, E_{\gamma_2} \geq 30\text{--}40$ MeV), it is possible to neglect, in Eq. (2), $|\rho(k_1 + k_2)|$ with respect to $|\rho(k_1 - k_2)|$ and, hence, the correlation function can be rewritten as

$$C_2(\vec{k}_1, \vec{k}_2) = \frac{1}{4} [1 + (\hat{\mathbf{k}}_1 \cdot \hat{\mathbf{k}}_2)^2] |\rho(k_1 - k_2)|^2. \quad (3)$$

In order to obtain numerical estimates of the photon correlation function, we assumed, as usual [11], the space-time density as a spherically symmetric Gaussian function with uncorrelated space and time coordinates:

$$\rho(r, t) = \frac{1}{4\pi^2 R^3 \tau} \exp(-r^2/2R^2 - t^2/2\tau^2), \quad (4)$$

where R and τ characterize the source radius and lifetime, respectively. Taking the four-dimensional Fourier transform of Eq. (4), it is possible to express Eq. (3) in terms of the observables $q_{\text{rel}} = |\vec{p}_{\gamma_1} - \vec{p}_{\gamma_2}|$ and $q_0 = |E_{\gamma_1} - E_{\gamma_2}|$ ($c = 1$):

$$C_2(q_{\text{rel}}, q_0) = \frac{1}{4} (1 + \cos^2 \theta_{\text{rel}}) \exp\left(-\frac{q_{\text{rel}}^2 R^2}{\hbar^2}\right) \exp\left(-\frac{q_0^2 \tau^2}{\hbar^2}\right) \quad (5)$$

(θ_{rel} being the relative angle between the two photons). This is the form used in all simulations described in the following.

Many samples of correlated events have been generated for various values of R and τ . In each of these events two photons, both having an energy larger than 30 MeV, have been emitted in the laboratory frame in accordance with a double differential cross section given by [6]:

$$\left. \frac{d^2\sigma}{d\Omega dE} \right|_{\text{lab}} \propto \frac{1}{Z} \left(1 - \alpha + \alpha \frac{\sin^2 \theta_{\text{lab}}}{Z^2}\right) \exp\left(-\frac{ZE_{\text{lab}}}{E_0}\right), \quad (6)$$

where

$$Z = \gamma(1 - \beta_s \cos \theta_{\text{lab}}) \quad (7)$$

and

$$\gamma = (1 - \beta_s^2)^{-1/2}. \quad (8)$$

The quantity $\beta_s = v_s/c$ indicates the photon source velocity in the laboratory frame, E_0 is the inverse slope parameter in the source frame, and α accounts for the dipolar character of the photon angular distribution from neutron-proton collisions. In our calculations β_s , E_0 , and α have been taken from the results of the best fit of the inclusive photon spectra [6]. The correlation between couples of photons has been imposed through Eq. (5) using a Monte Carlo technique.

Generally, both geometrical and physical limitations of real detectors prevent the complete knowledge of the full six-dimensional two-particle distribution reported in Eq. (1). Thus, the photon correlation function relative to filtered events cannot be constructed from the ratio given in that equation. In practice, the six-dimensional two-particle correlation function $P(\vec{k}_1, \vec{k}_2)$ is projected on an one- or, at most, two-dimensional one, $P(\vec{k}_1, \vec{k}_2) \rightarrow A(q_1), A'(q_1, q_2)$, where q_i are the so-called correlation observables. In our simulations we have used both the relative momentum q_{rel} and the relative energy q_0 . They are the most natural choices since the emitting source has been parametrized through Eq. (5). To evaluate the quantity $C(q)$, the correlation term $A(q)$ is then compared to a similar projection of some background sample $B(q)$, so that the experimental correlation function is given by

$$C(q) = \frac{A(q)}{B(q)}. \quad (9)$$

The uncorrelated term $B(q)$ is usually evaluated either starting from inclusive events, advisable when they are available, or using the event mixing technique [12], i.e., creating artificial pairs by combining single particles coming from randomly chosen two-particle correlated events. In this work we have adopted the first method. This approach may be justified considering that, in reactions between heavy ions producing photons in the intermediate energy regime, the mean value of the inclusive high-energy photon multiplicity (leaving out the case of no detected photon) is very close to 1 and, thus, the residual two-particle correlations are negligible.

Typical correlation functions $C(q_{\text{rel}})$ and $C(q_0)$ of simulated events filtered through the BaF₂ ball of the MEDEA multidetector are shown in Figs. 7 and 8, respectively, for a given couple of values of the source parameters ($R = 5$ fm and $\tau = 10$ fm/c). As we are interested here only in the effect of the experimental filter on the photon-photon correlation function, those pairs of photons coming from the neutral pion decay have not been included in the simulations (see next subsection for this). In both figures, solid lines are relative to the results of a best-fit procedure using the Gaussian functions

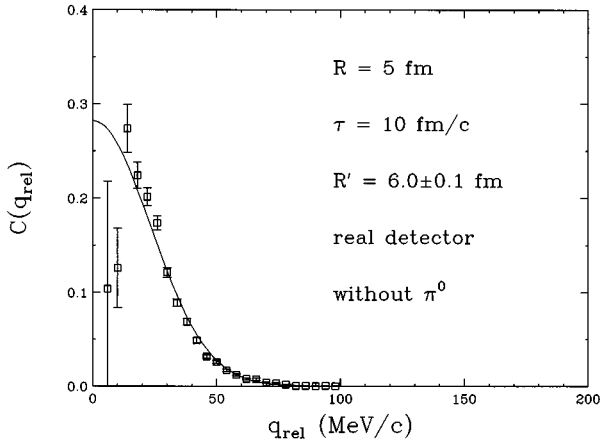


FIG. 7. Correlation function $C(q_{\text{rel}})$ for photons emitted from a source with $R=5$ fm and $\tau=10$ fm/c. The events are filtered through the BaF₂ ball of MEDEA. Photons from neutral pion decay are not included into the simulation.

$$C(q_{\text{rel}}) = A_{q_{\text{rel}}} \exp\left(-\frac{q_{\text{rel}}^2 R'^2}{\hbar^2}\right) \quad (10)$$

and

$$C(q_0) = A_{q_0} \exp\left(-\frac{q_0^2 \tau'^2}{\hbar^2}\right). \quad (11)$$

The aforementioned experimental limitation in the relative angle between photons, $\theta_{\text{rel}} \geq 15^\circ$, and the energy threshold $E_{\gamma_1}, E_{\gamma_2} > 30$ MeV makes it impossible to measure relative momenta smaller than about 7.5 MeV/c and strongly reduces the detection efficiency up to $q_{\text{rel}}=10-15$ MeV/c. Thus, only the points with $q_{\text{rel}} > 15$ MeV/c have been taken into account in the fitting procedure.

In this most general case of randomly oriented couples of photons the quantity q_{rel} is different from q_0 and the polarization term $(1 + \cos^2 \theta_{\text{rel}})$ in Eq. (5) changes on an event-by-

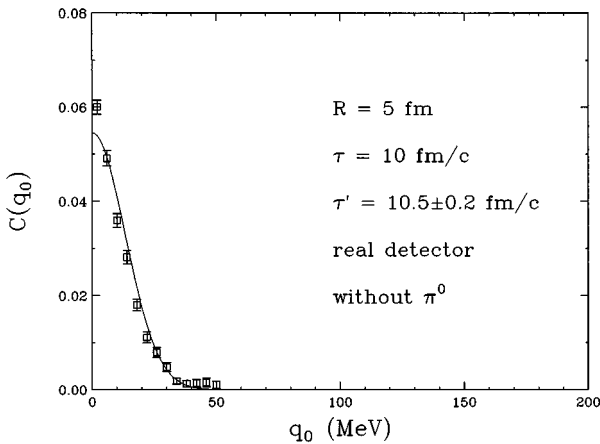


FIG. 8. Correlation function $C(q_0)$ for photons emitted from a source with $R=5$ fm and $\tau=10$ fm/c. The events are filtered through the BaF₂ ball of MEDEA. Photons from neutral pion decay are not included into the simulation.

event basis in a very complicated manner. To help in understanding, Fig. 9 shows the simulated two-dimensional correlation function $C_2(q_{\text{rel}}, q_0)$ for photons coming from a source with $R=5$ fm and $\tau=10$ fm/c and detected by an ideal detector (namely, 4π sr solid angle, infinite granularity, infinite angular resolution, no thresholds, perfect photon-charged particle and photon-neutron separation, no neutral pion background, complete cosmic-ray rejection, etc.). The condition $q_{\text{rel}}^2 \geq q_0^2$ ($c=1$), which must hold for real particles, makes the distribution not symmetric with respect to the $q_{\text{rel}}=q_0$ plane. The value of 0.5, expected for the maximum of the correlation function, is well reproduced and the widths of the distribution, from q_0 and q_{rel} directions (see Fig. 9, lower panels), are in agreement with the input values of R and τ . On the contrary, if one reports the quantities $C(q_{\text{rel}})$ and $C(q_0)$ (as in Figs. 7 and 8), through an implicit integration process over the not-used variable, both maxima and widths are not reproduced, notwithstanding the shape remaining roughly (but not exactly) Gaussian. Both R' and τ' are larger than R and τ , erroneously indicating a source with space-time size larger than the real one. This is a crucial point in the intensity interferometry technique. In order to extract from data reliable values of source sizes and lifetimes, one can either directly fit the bidimensional correlation function $C_2(q_{\text{rel}}, q_0)$ or the two monodimensional distributions $C(q_{\text{rel}})$ and $C(q_0)$. The application of the first method needs very good statistics, often unrealistic in actual experiments. The second method is more suitable, as it is shown Ref. [8], even if it involves nested integrations of the asymmetric $C_2(q_{\text{rel}}, q_0)$. In any case, however, the results must be considered with great care. Both the relative angle term in the correlation function and the detector efficiency make R' and τ' different from the real source parameters, although they are correlated to them. Only through a complete simulation is it possible to find the relations between these widths and the true R and τ values. This point will be discussed with much greater detail in Sec. IV.

B. Response to the background

1. Neutral pions

The most important source of background in photon-photon correlation experiments is represented by neutral pions whose production cross section is a sizable fraction of the hard-photon cross section at these bombarding energies [13]. As stated in Sec. II, neutral pions are detected through the simultaneous recording of the two photons coming from their main decay channel. Figure 10 shows a simulated invariant mass distribution obtained with the real detector. Dots refer to the spectrum reconstructed only with the energies deposited in the two central detectors, while the solid line is the results obtained including the information coming from the two surrounding clusters defined in Sec. III A 1. Figure 11 shows, as an example, the comparison between the invariant mass distribution obtained by the BaF₂ ball of MEDEA from the $^{36}\text{Ar}+^{27}\text{Al}$ reaction at 95 MeV/nucleon and that simulated by GEANT3. The full width at half maximum (FWHM) of the distribution is about 18% of the neutral pion rest mass ($m_{\pi^0}=135$ MeV). In order to give an idea of the degree of accuracy in the knowledge of the detector efficiency for pions, the comparison between a realistic input

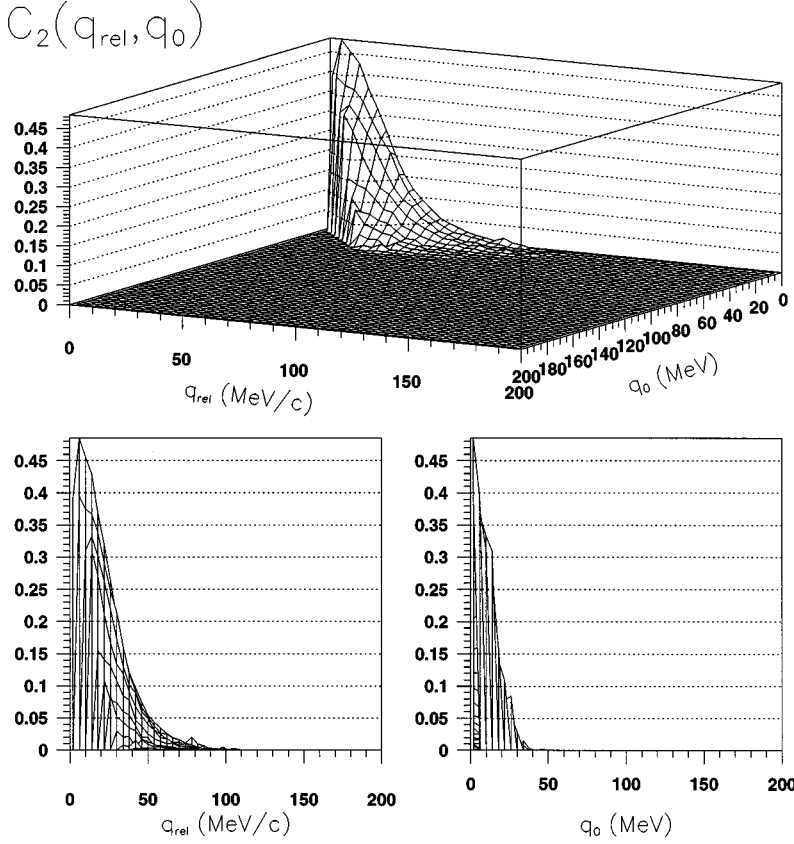


FIG. 9. Bidimensional correlation function $C_2(q_{\text{rel}}, q_0)$ for photons emitted from a source with $R=5$ fm and $\tau=10$ fm/c (upper panel). In the lower panels the views from the q_{rel} and q_0 axes are reported. The events are filtered through an ideal detector.

pion spectrum and that reconstructed after filtering through the detector is shown in Fig. 12. As has been shown in Sec. II, neutral pions can then be easily identified within, and eventually subtracted from, the ensemble of two-photon events imposing bidimensional conditions on the experimental distributions of the relative angle and invariant mass of the two photons as functions of their total energy.

The background due to the neutral pion main decay channel has been taken into account by also including, in the simulated correlated events, pairs of photons coming from

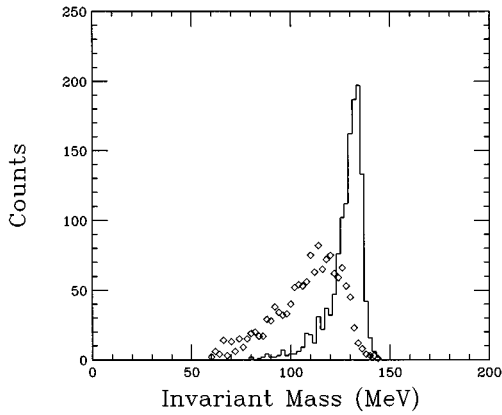


FIG. 10. Invariant mass spectrum of neutral pions coming from GEANT3 simulations. Dots refer to the spectrum reconstructed only with the energies deposited in the two central detectors, while the solid line is the results obtained including the information coming from the two surrounding clusters.

the π^0 decay. The pion source has been treated in the usual framework of a moving source parametrization using the following analytic form of the double-differential cross section [14]:

$$\left(\frac{d^2\sigma}{d\Omega dE} \right)_{\text{lab}} = pE' \frac{d^2\sigma}{p'^2 dp' d\Omega'}, \quad (12)$$

where

$$E' = \gamma(E - \beta_0 p \cos\theta_{\text{lab}}), \quad (13)$$

$$\gamma = (1 - \beta_0^2)^{-1/2}, \quad (14)$$

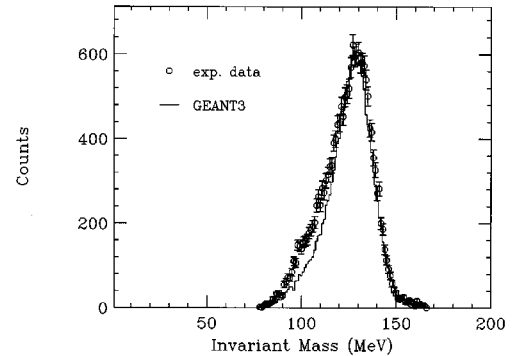


FIG. 11. Comparison between the invariant mass distribution obtained by the BaF₂ ball of MEDEA from the $^{36}\text{Ar}+^{27}\text{Al}$ reaction at 95 MeV/nucleon and that simulated by GEANT3 taking into account all physical and geometrical characteristics of the detector.

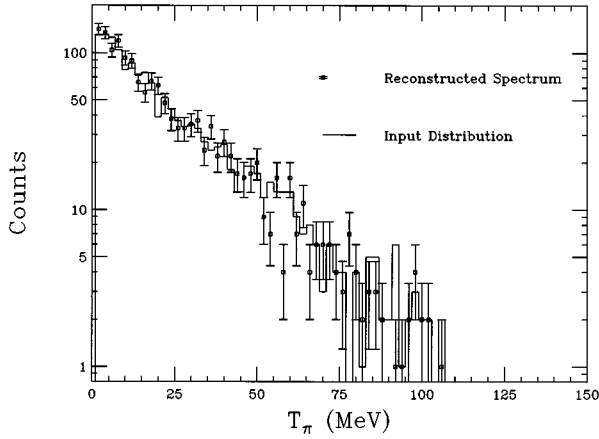


FIG. 12. Comparison between a realistic input pion spectrum and that reconstructed after filtering through the detector.

and

$$\frac{d^2\sigma}{p'^2 dp' d\Omega'} \propto \frac{1}{4\pi m^3} \frac{e^{-t'/\tau}}{2(\tau/m)^2 K_1(m/\tau) + (\tau/m) K_0(m/\tau)}. \quad (15)$$

E , p , E' , and p' are the pion total energies and linear momenta in the laboratory and source frame, respectively. θ_{lab} is the detection angle in the laboratory frame and m is the rest mass of the neutral pion. K_0 and K_1 are the modified Bessel functions of order 0 and 1, respectively, also known as MacDonald functions [15]. The source parameters are represented by the slope parameter τ and the velocity of the source in the laboratory frame, β_0 . In our simulations we used the values of β_0 and τ extracted from the best fit of the measured inclusive spectra [6]. In order to take into account the measured values of the pion (σ_π) and hard-photon (σ_γ) total production cross sections [6], a *neutral pion* event (two correlated photons coming from the π^0 decay) has been generated every σ_γ/σ_π uncorrelated inclusive events. As an example, Figs. 13 and 14 show the filtered correlation functions $C(q_{\text{rel}})$ and $C(q_0)$ for simulated events containing also couples of photons coming from π^0 decays. In order to compare the results, the same input source parameters ($R=5$ fm and $\tau=10$ fm/c) have been chosen. The neutral pion signal is confined in the high-relative-momentum part of the $C(q_{\text{rel}})$ spectrum and its presence does not affect significantly the determination of R' . On the contrary, it is distributed practically everywhere in the $C(q_0)$ distribution, completely destroying the information about the lifetime of the emitting source. This information can be, however, recovered. In fact, Fig. 15 shows the $C(q_0)$ correlation function under the condition $q_{\text{rel}} < 70$ MeV/c which rejects those photons coming from the π^0 decay. As one can see, the time correlation signal is restored and τ' turns out to be the same of that extracted from data without neutral pion contamination. The fact that the shape of the $C(q_0)$ correlation function becomes approximately Gaussian has been verified for many different but realistic cuts on q_{rel} .

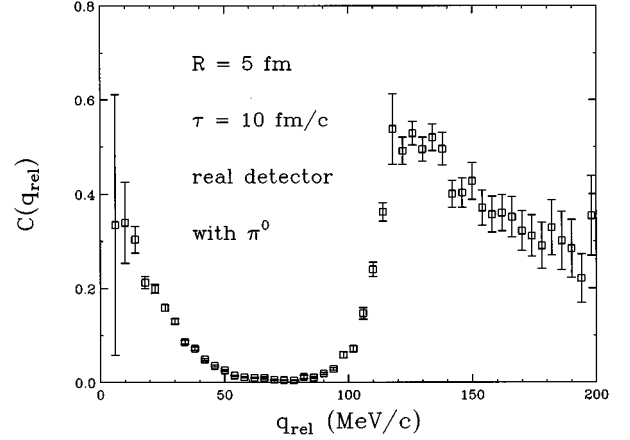


FIG. 13. Correlation function $C(q_{\text{rel}})$ for photons emitted from a source with $R=5$ fm and $\tau=10$ fm/c. The events are filtered through the BaF₂ ball of MEDEA. Photons from neutral pion decay are included into the simulation.

2. γ - γ^{π^0} events

Another source of noise, related to neutral pion decay, is associated to those two-photon events where only one photon comes from the source under investigation and the other one from a π^0 decay not completely detected due, for example, to the geometrical efficiency of the real detector. This process, involving the existence of $\gamma \cap \pi^0$ coincidence events, is a second-order one with respect to that discussed before, but its contribution cannot be *a priori* neglected because it is related to the unknown cross section ratio $\sigma(\gamma_1 \cap \gamma_2, E_{\gamma_1, \gamma_2} > 30 \text{ MeV}) / \sigma(\gamma \cap \gamma^{\pi^0}, E_{\gamma, \gamma^{\pi^0}} > 30 \text{ MeV})$.

In spite of the fact that it is thus impossible to put this kind of event into the same set of all correlated events and look at the resulting correlation function, we have anyway evaluated its contribution in the relative momentum and energy distributions $A(q_{\text{rel}})$ and $A(q_0)$ of the two photons. As an ex-

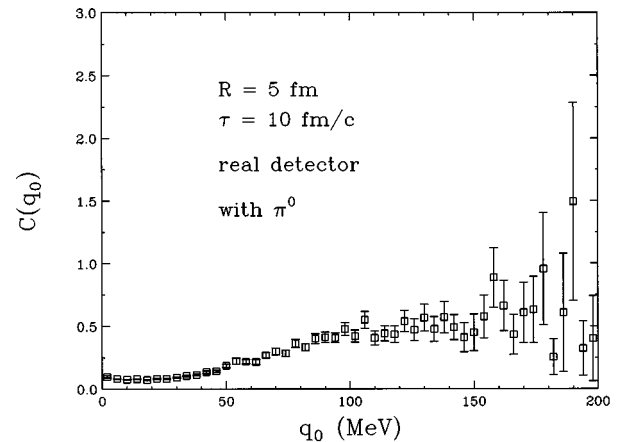


FIG. 14. Correlation function $C(q_0)$ for photons emitted from a source with $R=5$ fm and $\tau=10$ fm/c. The events are filtered through the BaF₂ ball of MEDEA. Photons from neutral pion decay are included into the simulation.

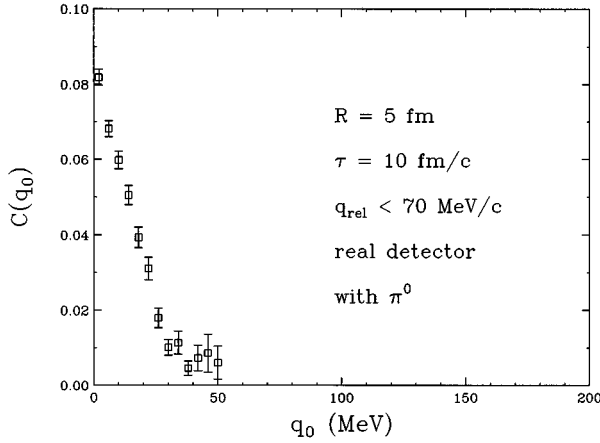


FIG. 15. Correlation function $C(q_0)$ for photons emitted from a source with $R=5$ fm and $\tau=10$ fm/c satisfying the condition $q_{\text{rel}} < 70$ MeV/c. The events are filtered through the BaF₂ ball of MEDEA. Photons from neutral pion decay are included into the simulation.

ample, Fig. 16 shows the comparison between the $A(q_{\text{rel}})$ filtered distribution of γ - γ correlated events ($R=5$ fm and $\tau=10$ fm/c, upper panel) and that one of γ - γ^{π^0} events (lower panel). Independently of the relative weights, the two spectra are located in different ranges of the relative momentum and, hence, the two contributions can be quite easily identified and separated.

3. Cosmic rays

The noise induced in the photon-photon correlation signal by the cosmic radiation arises from the fact that cosmic muons, traversing the modules of a real photon multidetector, can originate inside it couples completely similar to those due to the photons coming from the target. In order to study this background, a large number of μ mesons (about 10^6) have been generated and their interaction with

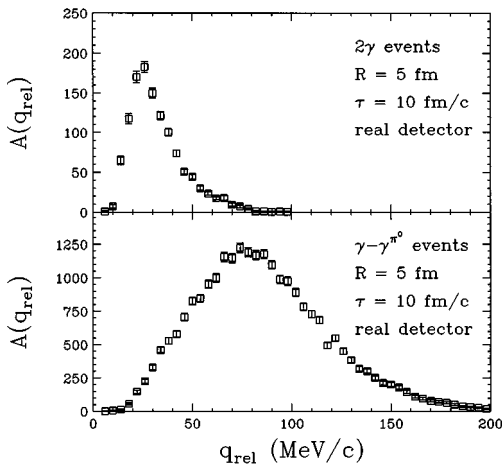


FIG. 16. Filtered relative momentum distributions of γ - γ correlated events ($R=5$ fm and $\tau=10$ fm/c, upper panel) and γ - γ^{π^0} events (lower panel; see text).

the BaF₂ ball of the MEDEA multidetector has been studied by means of full GEANT3 simulations [8,9]. Cosmic muons have been created with a kinetic energy of 2 GeV, which represents a realistic mean energy of the muon flux at sea level [16], and with an angular distribution proportional to $\cos^2\theta$, where θ is the minimum angle between the muon momentum and the vertical direction. Only those events generating two showers inside the BaF₂ ball of MEDEA, each having a total deposited energy greater than 30 MeV, have been considered for further analysis. The percentage of this kind of filtered events over the total number of generated ones was about 25%. Taking into account the absolute cosmic-ray intensity at sea level (without the correction due to the geomagnetic latitude of the experimental site) and the dimensions of the detector, it is straightforward to calculate a value of the total expected cosmic rate of about 200–250 Hz. Considering that, because of the time resolution of the BaF₂ modules, all photons coming from the target are generally gathered in about 2 ns, over realistic total coincidence windows of about 80–100 ns, the expected cosmic rate under the “photon peak” is 4–5 Hz. Taking also into account that the probability of a cosmic muon to be detected as two distinct showers, each having an energy larger than 30 MeV, is about 25% on the average, the final rate of the real cosmic background in the process under study is about 1–2 Hz. This number has to be compared with 1.8 π^0 per second detected in the $^{27}\text{Al}(^{36}\text{Ar}, \pi^0)$ reaction at 95 MeV/nucleon. Fortunately, this huge contribution can be reduced to a negligible value simply by imposing the detection of charged particles in coincidence with photons. In fact, unlike fast plastic scintillators, barium fluoride detectors exhibit typical recovery times in the order of 1 μs . Thus, in order to avoid undesired pileup effects, the beam currents are usually limited to having not more than 10^4 reactions per second. This means that, if one works with a typical total coincidence window of about 100 ns, only one beam pulse over 10^3 contains a physical reaction. Considering also the dead time of the data acquisition system, the expected cosmic rate in the BaF₂ ball, after imposing the $\nu > 0$ condition, decreases to about 3×10^{-4} Hz. Although this value is very small, the cosmic radiation background could, however, still represent a problem for very long runs as those necessary for photon-photon correlation measurements. In order to investigate this subject, we reconstructed from simulated events the relative momentum and energy distributions $A(q_{\text{rel}})$ and $A(q_0)$ of the two photons generated from a cosmic muon. Figure 17 shows the comparison between the $A(q_{\text{rel}})$ filtered distribution of γ - γ correlated events ($R=5$ fm and $\tau=10$ fm/c, upper panel) and that of two-shower cosmic events (lower panel). Also, in this case, independently of the absolute normalization, the two spectra are located in very different ranges of the relative momentum. Hence, the couples of showers coming from cosmic radiation, even if they are present, cannot modify at all the information contained in the photon-photon correlation function.

4. γ conversion

Barium fluoride scintillators are in principle also sensitive, by their nature, to the e^+e^- pairs coming from γ conversion which could represent a background in the study of photon-photon correlation. Because of the fact that all the

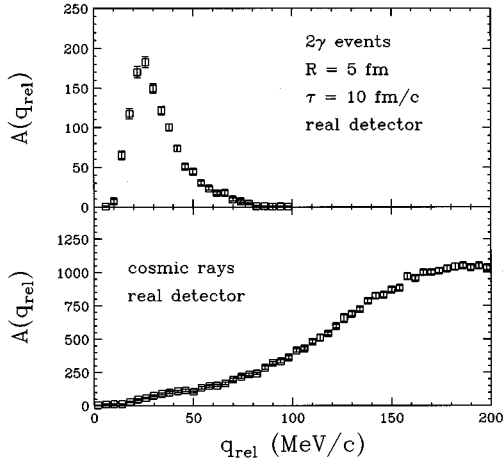


FIG. 17. Filtered relative momentum distributions of $\gamma\text{-}\gamma$ correlated events ($R=5$ fm and $\tau=10$ fm/c, upper panel) and two-shower cosmic events (lower panel).

MEDEA multidetector operates in a vacuum, inside a big scattering chamber [3], the only possible sources of γ conversion are the target and a thin layer of Teflon and aluminized Mylar, 200 μm thick, which wraps each module [3]. The pair production cross section [4] for photons having an energy greater than 60 MeV (the minimum one to produce two 30 MeV showers) takes values in the range of 0.01–1 μb for all possible atomic numbers. This means that, taking into account the target thicknesses used in this experiment and the total yield of more than 60 MeV photons, the probability that a e^+e^- pair can be produced inside the target is about 10^{-8} . The number of e^+e^- pairs generated in the layers of Teflon and aluminized Mylar could be considerably larger but, since the two particles are in this case produced very close to one (and only one) scintillator, the condition on the minimum relative detection angle ($\theta_{\text{rel}} \geq 15^\circ$) reduces near to zero the probability that γ conversion could originate two distinct showers into the detector.

IV. RESULTS

The relative momentum distribution of all two-photon events detected in the reaction $^{36}\text{Ar}+^{27}\text{Al}$ at 95 MeV/nucleon is reported in Fig. 18. Solid circles refer to those couples of photons coming from π^0 decay, i.e., standing inside the contours drawn in Fig. 4, while open circles refer to those couples of photons standing outside the contours drawn in Fig. 4. These latter pairs of photons, producing the large bump centered around 80–100 MeV/c, are relative both to ‘‘badly’’ detected pions (the tail of the invariant mass distribution reported in Fig. 11) and to $\gamma\text{-}\gamma^{\pi^0}$ events (see lower panel of Fig. 16). True $\gamma\text{-}\gamma$ events are expected to place themselves in the lowest part of the relative momentum spectrum. The absence of values of q_{rel} lower than about 10 MeV/c is due to the limitation imposed both in the minimum energy and relative angle of the two detected photons.

In order to evaluate the correlation function, the relative momentum distribution plotted in Fig. 18 has been divided by that obtained folding the inclusive photon events through the event-mixing technique [12]. The normalization factor

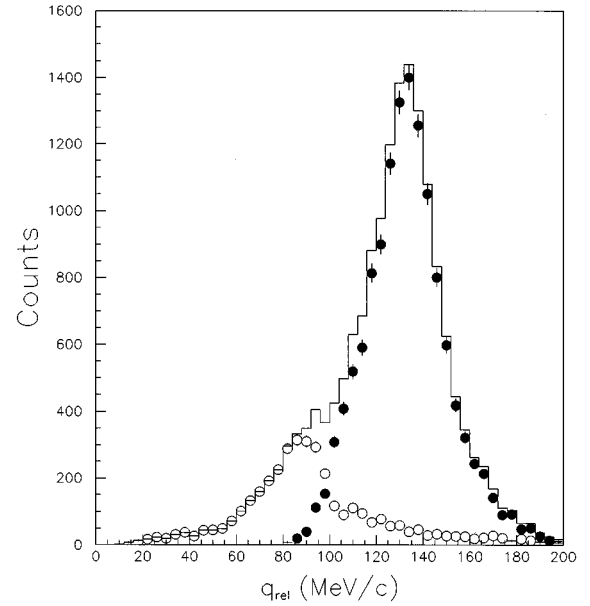


FIG. 18. Relative momentum distribution of two-photon events detected in the $^{36}\text{Ar}+^{27}\text{Al}$ reaction at 95 MeV/nucleon (solid histogram). Solid circles refer to those pairs of photons coming from π^0 decay, i.e., standing inside the contours drawn in Fig. 4, while open circles refer to those pairs of photons standing outside.

takes explicitly into account the different run times of the two sets of events. The correlation distribution $1 + C(q_{\text{rel}})$, as a function of the relative momentum, is reported in the upper panel of Fig. 19. The three above-cited contributions are visible: a peak, due to neutral pions (centered around 140 MeV/c), a large bump, due to ‘‘badly’’ measured pions and to $\gamma\text{-}\gamma^{\pi^0}$ events (between 50 and 150 MeV/c), and the photon-photon correlation signal (for $q_{\text{rel}} < 45$ MeV/c). The solid line passing through the points refers to the result of a

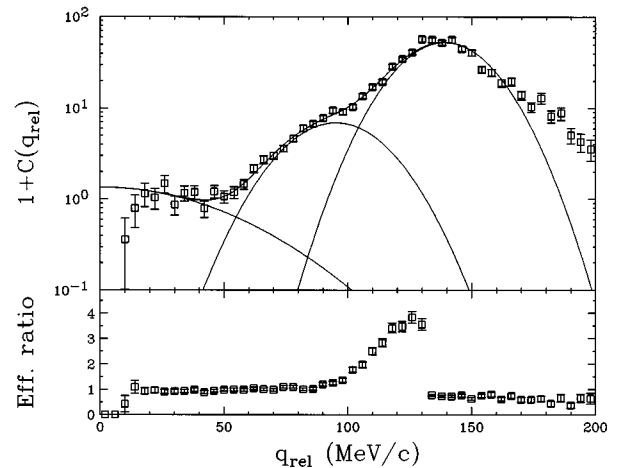


FIG. 19. Upper panel: correlation distribution $1 + C(q_{\text{rel}})$, as a function of the relative momentum, for the pairs of photons detected in the $^{36}\text{Ar}+^{27}\text{Al}$ reaction at 95 MeV/nucleon. Solid curves are relative to the result of a best-fit procedure (see text). Lower panel: corresponding detector efficiency.

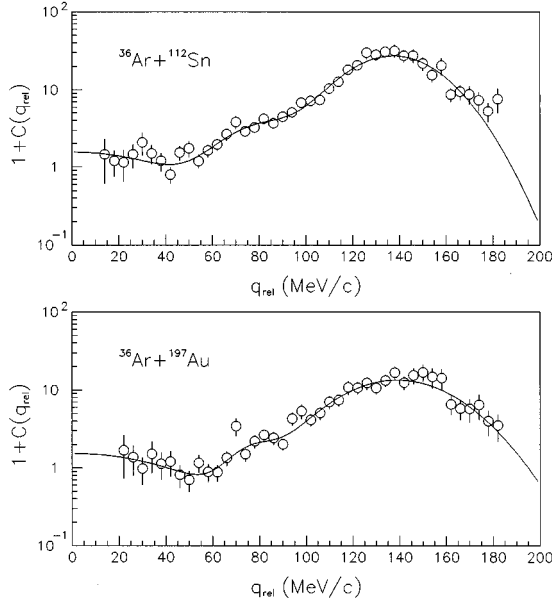


FIG. 20. Correlation distribution $1 + C(q_{\text{rel}})$, as a function of the relative momentum, for the pairs of photons detected in the $^{36}\text{Ar} + ^{112}\text{Sn}$ (upper panel) and $^{36}\text{Ar} + ^{197}\text{Au}$ (lower panel) reactions at 95 MeV/nucleon.

best-fit procedure using the sum of three Gaussian functions ($c=1$):

$$C(q_{\text{rel}}) = \lambda_R e^{-q_{\text{rel}}^2 R'^2 / \hbar^2} + A_1 e^{-(q_{\text{rel}} - q_1)^2 / 2\sigma_1^2} + A_2 e^{-(q_{\text{rel}} - q_2)^2 / 2\sigma_2^2}, \quad (16)$$

one for each component. R' is the width of the spatial correlation signal. Other curves in the same figure refer to each of the three contributions. For the sake of correctness, the first two points in the correlation distribution, having $q_{\text{rel}} < 15$ MeV/c, have been not included in the fitting because the evaluated detector efficiency for this correlation function, reported in the lower panel of Fig. 19, shows a steep falloff to zero below that value of the relative momentum. An efficiency greater than 1 is not surprising as it is defined as the ratio between the detector efficiencies for the numerator and the denominator of the correlation function defined in Eq. (9) [8]. The relative-momentum correlation functions for the other two used targets are reported in Fig. 20. The extracted values of the width R' are summarized, for all targets, in the second column of Table I.

The correlation distributions $C(q_0)$, as functions of the relative energy, are plotted, for the various targets, in Figs.

TABLE I. Values of the measured source parameters R' and τ' and those of the extracted ones R and τ , for the various studied systems.

System	R' (fm)	R (fm)	τ' (fm/c)	τ (fm/c)
$^{36}\text{Ar} + ^{27}\text{Al}$	3.1 ± 1.2	0.8 ± 0.4	2.6 ± 1.7	2.0 ± 1.0
$^{36}\text{Ar} + ^{112}\text{Sn}$	4.0 ± 1.4	1.7 ± 0.7	6.1 ± 1.4	6.3 ± 1.8
$^{36}\text{Ar} + ^{197}\text{Au}$	3.2 ± 1.0	2.2 ± 1.1	9.0 ± 1.9	9.9 ± 1.9

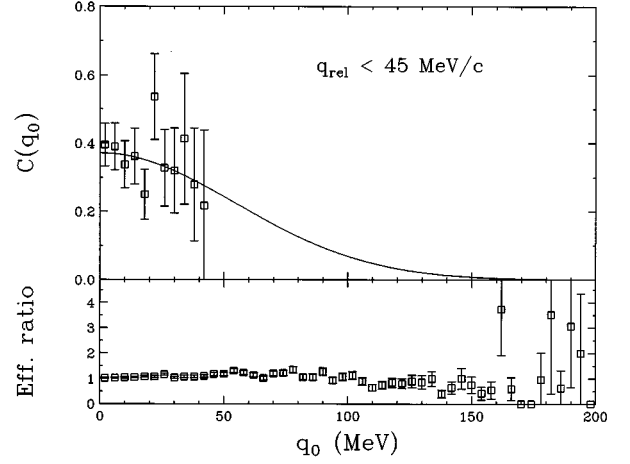


FIG. 21. Upper panel: correlation distribution $C(q_0)$, as a function of the relative energy, for the pairs of photons detected in the $^{36}\text{Ar} + ^{27}\text{Al}$ reaction at 95 MeV/nucleon and having $q_{\text{rel}} < 45$ MeV/c. Solid curve is relative to the result of a best-fit procedure (see text). Lower panel: corresponding detector efficiency.

21 and 22. Only those couples of photons having $q_{\text{rel}} < 45$ MeV/c have been taken into account to make those plots. The solid curves are the results of best-fit procedures using the function ($c=1$)

$$C(q_0) = \lambda_{\tau'} e^{-q_0^2 \tau'^2 / \hbar^2}, \quad (17)$$

where τ' is the width of the temporal correlation signal. In this case all the points have been included in the fitting due to the shape of the evaluated detector efficiency for this cor-

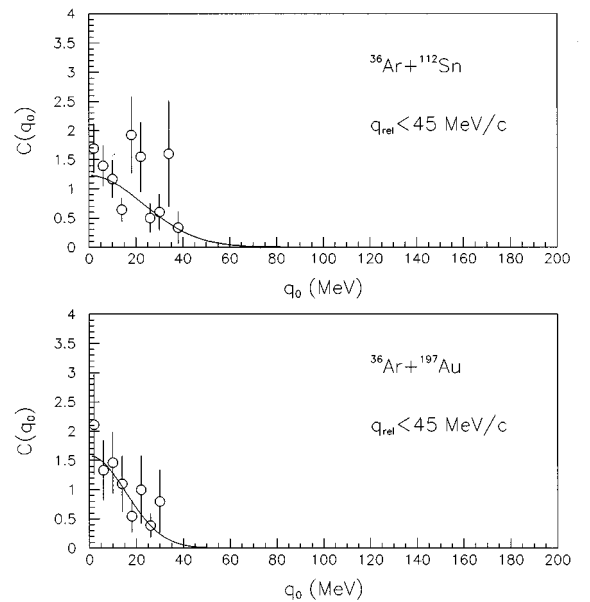


FIG. 22. Correlation distribution $1 + C(q_0)$, as a function of the relative energy, for the pairs of photons detected in the $^{36}\text{Ar} + ^{112}\text{Sn}$ (upper panel) and $^{36}\text{Ar} + ^{197}\text{Au}$ (lower panel) reactions at 95 MeV/nucleon and having $q_{\text{rel}} < 45$ MeV/c.

TABLE II. The values of the source parameters R and τ used as input of the simulation described in the text are reported together with those R' and τ' extracted from the best fit of the relative momentum and energy correlation functions after filtering through the detector. The data refer to the ^{27}Al target.

R (fm)	τ (fm/c)	R' (fm)	τ' (fm/c)
0.5	1	2.94 ± 0.51	1.93 ± 1.11
0.5	2	3.15 ± 0.47	2.89 ± 0.78
0.5	3	2.86 ± 0.23	3.36 ± 0.25
0.5	5	3.25 ± 0.19	4.89 ± 0.17
1	5	3.55 ± 0.22	4.90 ± 0.16
1.5	1	4.11 ± 0.55	2.61 ± 0.73
1.5	2	3.17 ± 0.24	2.02 ± 0.91
1.5	3	3.15 ± 0.20	3.79 ± 0.46

relation function which is reported, for the ^{27}Al target, in the lower panel of Fig. 21. The extracted values of the width τ' are summarized, for all targets, in the fourth column of Table I. It is worth noting that, changing the value of the upper threshold of q_{rel} in the realistic relative momentum region between 40 and 50 MeV/c, all of the extracted values of τ' resulted in being consistent among themselves within their error bars.

As has been discussed in detail in Ref. [8] and reported here in Sec. III A 2, the distortion effect due to the interference between the polarizations of the two emitted photons, always present in the correlation function, and that due to the detector efficiency make R' and τ' different from the real source parameters. These effects are also not simply additive and operate at the same time in a very complicated way depending both on the values of the source parameters and on the detector geometry. So in order to unfold the searched values of R and τ from the measured ones of R' and τ' we performed a lot of full GEANT3 simulations of the detection of pairs of correlated photons by the BaF₂ ball of the MEDEA multidetector and we submitted the simulated events to the same analysis technique described and used for experimental data. Some input values of the source parameters R and τ (close to the region of interest) together with the corresponding output ones R' and τ' , extracted from the best fit of the simulated correlation functions $C(q_{\text{rel}})$ and $C(q_0)$ (after filtering through the detector), are reported in Tables II–IV for the various targets. Owing to the fact that the interesting regions of the planes (R, τ) are quite small and the chosen grids in those planes are rather close, we

TABLE III. The same as Table II for the ^{112}Sn target.

R (fm)	τ (fm/c)	R' (fm)	τ' (fm/c)
1	10	4.48 ± 0.20	8.99 ± 0.20
1.5	3	3.15 ± 0.20	3.79 ± 0.46
1.5	5	3.66 ± 0.15	4.92 ± 0.16
1.5	10	4.12 ± 0.12	8.67 ± 0.17
2	5	4.02 ± 0.12	5.01 ± 0.15
2	10	4.50 ± 0.11	8.91 ± 0.18
3	5	4.38 ± 0.11	4.99 ± 0.15
3	10	5.01 ± 0.09	8.78 ± 0.16

TABLE IV. The same as Table III for the ^{197}Au target.

R (fm)	τ (fm/c)	R' (fm)	τ' (fm/c)
1.5	3	3.15 ± 0.20	3.79 ± 0.46
1.5	5	3.66 ± 0.15	4.92 ± 0.16
1.5	10	4.12 ± 0.12	8.67 ± 0.17
2	5	4.02 ± 0.12	5.01 ± 0.15
2	10	4.50 ± 0.11	8.91 ± 0.18
3	5	4.38 ± 0.11	4.99 ± 0.15
3	10	5.01 ± 0.09	8.78 ± 0.16
4	10	4.08 ± 0.37	9.96 ± 0.33

expanded the unknown functions $R(R', \tau')$ and $\tau(R', \tau')$ as second-order polynomials whose free parameters have to be fitted to the values of R' and τ' extracted from simulated data. So the problem of finding R and τ for the three studied systems reduces to an interpolation of $R(R', \tau')$ and $\tau(R', \tau')$. The extracted values of R and τ are reported in the third and fifth columns of Table I for the various targets. It is worth noting that the values of R and τ for the ^{27}Al target are consistent, within the statistical uncertainties, to those extracted in Ref. [2] where first-order functions of R' and τ' were used.

As has been pointed out in Ref. [10], however, the numeric value of R represents only one (the other is τ) of the σ values of the assumed space-time distribution of the source and it is, hence, not directly comparable with any observable. A more reliable quantity is the root-mean-squared radius r_{rms} , which, in the hypothesis of a spherical symmetric source, is written as

$$r_{\text{rms}} = \sqrt{\langle \vec{r} \cdot \vec{r} \rangle} = \sqrt{3}R. \quad (18)$$

The values of r_{rms} for the three studied system are reported in the second column of Table V. In heavy-ion collisions at around 100 MeV bombarding energy, hard photons are thought to come from incoherent nucleon-nucleon collisions which take place, in the very first phase of the reaction, within the overlap region between the two nuclei [17]. Using the geometrical estimation [18] of the number (averaged over the impact parameter) of the participant nucleons producing two hard photons,

$$\langle N_{pn} \rangle_{\gamma\gamma} \equiv \langle N_{pn}(N_{pn} - 1) \rangle_b \quad (19)$$

(where N_{pn} is the number of first proton-neutron collisions), it is possible to calculate the Gaussian radius [19] of the two-nuclei overlap zone through the formula

$$R_{\text{ov}} = \sqrt{\frac{2}{5}} (1.2 \langle N_{pn} \rangle_{\gamma\gamma})^{1/3}. \quad (20)$$

TABLE V. The values of the root-mean-squared radius r_{rms} are compared, for the three studied systems, with those of the overlap radius R_{ov} and those of the total radius R_{tot} .

System	r_{rms} (fm)	R_{ov} (fm)	R_{tot} (fm)
$^{36}\text{Ar} + ^{27}\text{Al}$	1.4 ± 0.7	1.95	7.56
$^{36}\text{Ar} + ^{112}\text{Sn}$	3.0 ± 1.2	3.00	9.75
$^{36}\text{Ar} + ^{197}\text{Au}$	3.8 ± 1.9	3.35	10.94

The values of R_{ov} for the three systems are reported in the third column of Table V. The agreement with the r_{rms} 's is very good. Furthermore, both series of values are very much different from the sums of projectile and target radii $R_{tot}=1.2(A_p^{1/3}+A_t^{1/3})$ which are reported for comparison in the last column of Table V. Our data are also in agreement with much more refined calculations based on the resolution of microscopic transport equations. In a recent paper, in fact, Barz *et al.* [20] have successfully reproduced the experimental correlation functions relative to the ^{27}Al target with a Boltzmann-Uehling-Uhlenbeck (BUU) calculation based on first-chance nucleon-nucleon collisions.

V. SUMMARY AND CONCLUSIONS

The chaoticity and the strong space-time localization of the source emitting high-energy photons in heavy-ion collisions at intermediate energies, foreseen by present microscopic theoretical models [17], allow and justify the use of the intensity interferometry technique as a method of analysis of experimental data aiming to provide valuable information, both on the geometry and dynamics of the collision, in an almost model-independent way.

In this article we have exploited the HBT effect for an extensive study of photon-photon correlation data relative to the reactions $^{36}\text{Ar}+^{27}\text{Al}$, $^{36}\text{Ar}+^{112}\text{Sn}$, and $^{36}\text{Ar}+^{197}\text{Au}$ at 95 MeV/nucleon and obtained with the BaF₂ ball of the MEDEA multidetector.

Great care has been devoted to a detailed evaluation, through realistic Monte Carlo simulations, of the detector response both to the signal under investigation and to the sources of background. A new method, also based on computer simulations, has been proposed and verified to get information both on the source size and lifetime.

Experimental results are in agreement and validate the picture of the hard-photon production mechanism due to first, single, and incoherent nucleon-nucleon collisions. The values of the spatial size of the source, for the various systems, are in fact very small and compatible with the radii of the geometric overlap volumes between the two colliding nuclei. The source lifetimes are in agreement, at least for the lightest used target, with BUU calculations based on first-chance proton-neutron collisions. They steadily increase as a function of the target mass possibly due to the presence of projectile stopping effects which have already been observed for the same systems at the same bombarding energy [21].

-
- [1] For a review, see e.g., D. H. Boal, C. K. Gelbke, and B. J. Jennings, *Rev. Mod. Phys.* **62**, 553 (1990), and references therein; W. Bauer, C. K. Gelbke, and S. Pratt, *Annu. Rev. Nucl. Part. Sci.* **42**, 77 (1992), and references therein.
- [2] A. Badalà, R. Barbera, A. Palmeri, G. S. Pappalardo, F. Riggi, A. C. Russo, G. Russo, and R. Turrisi, *Phys. Rev. Lett.* **74**, 4779 (1995) and reference therein.
- [3] E. Migneco *et al.*, *Nucl. Instrum. Methods Phys. Res. A* **314**, 31 (1992).
- [4] CERN Application Software Group, *GEANT: Detector Description and Simulation Tool* (CERN, Geneva, 1993); CERN Program Library Long Writups W5013.
- [5] A. Badalà *et al.*, *Phys. Rev. C* **48**, 2350 (1993).
- [6] A. Badalà, R. Barbera, A. Palmeri, G. S. Pappalardo, F. Riggi, A. C. Russo, G. Russo, and R. Turrisi, *Phys. Rev. C* **55**, 2506 (1997), the preceding paper.
- [7] A. Badalà, R. Barbera, A. Palmeri, G. S. Pappalardo, F. Riggi, and A. C. Russo, *Nucl. Instrum. Methods Phys. Res. A* **306**, 283 (1991).
- [8] A. Badalà, R. Barbera, A. Palmeri, G. S. Pappalardo, F. Riggi, A. C. Russo, G. Russo, and R. Turrisi, *Nucl. Instrum. Methods Phys. Res. A* **351**, 387 (1994).
- [9] A. Badalà, R. Barbera, A. Palmeri, G. S. Pappalardo, F. Riggi, A. C. Russo, G. Russo, and R. Turrisi, *Nucl. Instrum. Methods Phys. Res. A* **357**, 443 (1995).
- [10] W. A. Zajc, in *Proceedings of a NATO Advanced Study Institute on Particle Production in Highly Excited Matter*, IL Ciocco, Italy, 1992, edited by H. H. Gutbrod and J. Rafelski (Plenum Press, New York, 1993).
- [11] D. Neuhauser, *Phys. Lett. B* **182**, 289 (1986).
- [12] D. Drijard, H. G. Fischer, and T. Nakada, *Nucl. Instrum. Methods Phys. Res. A* **225**, 367 (1984).
- [13] V. Metag, *Prog. Part. Nucl. Phys.* **30**, 75 (1993).
- [14] R. Barbera *et al.*, *Nucl. Phys.* **A518**, 767 (1993).
- [15] *Handbook of Mathematical Functions*, Applied Mathematics Series No. 55, edited by M. Abramowitz and I. A. Stegun (U.S. Department of Commerce, National Bureau of Standards, Washington, 1972).
- [16] M. Aguilar-Benitez *et al.*, *Phys. Lett. B* **239**, 1 (1990).
- [17] W. Cassing, V. Metag, U. Mosel, and K. Niita, *Phys. Rep.* **188**, 363 (1990).
- [18] H. Nifenecker and J. P. Bondorf, *Nucl. Phys.* **A442**, 478 (1985).
- [19] W. A. Zajc *et al.*, *Phys. Rev. C* **29**, 2173 (1984).
- [20] H. W. Barz, B. Kämpfer, Gy. Wolf, and W. Bauer, *Phys. Rev. C* **53**, R553 (1996).
- [21] A. Badalà, R. Barbera, A. Palmeri, G. S. Pappalardo, F. Riggi, A. C. Russo, G. Russo, and R. Turrisi, *Phys. Rev. C* **53**, 1782 (1996), and references therein.